

Local void vs dark energy: confrontation with WMAP and type Ia supernovae

To cite this article: Stephon Alexander *et al* JCAP09(2009)025

View the [article online](#) for updates and enhancements.

You may also like

- [INVERSE PROBLEMS NEWSLETTER](#)
- [Numerical Analysis Considering the Effects of Liquid Water on PEMFC Unsteady Performance](#)
Takanori Fukuda and Takuto Araki
- [NEWS](#)

Local void vs dark energy: confrontation with WMAP and type Ia supernovae

Stephon Alexander,^a Tirthabir Biswas,^a Alessio Notari^{b,c} and
Deepak Vaid^a

^aDepartment of Physics, Institute for Gravitation and the Cosmos,
The Pennsylvania State University,
104 Davey Lab, University Park, PA, 16802, U.S.A

^bPhysics Department, McGill University,
3600 University Road, Montréal, QC, H3A 2T8, Canada

^cCERN, Theory Division,
CH-1211 Geneva 23, Switzerland

E-mail: stephon@slac.stanford.edu, tbiswas@gravity.psu.edu,
notari@hep.physics.mcgill.ca, deepak@phys.psu.edu

Received April 2, 2009

Revised August 25, 2009

Accepted August 26, 2009

Published September 21, 2009

Abstract. It is now a known fact that if we happen to be living in the middle of a large underdense region, then we will observe an “apparent acceleration”, even when any form of dark energy is absent. In this paper, we present a “Minimal Void” scenario, i.e. a “void” with minimal underdensity contrast (of about -0.4) and radius ($\sim 200 - 250$ Mpc/ h) that can, not only explain the supernovae data, but also be consistent with the 3-yr WMAP data. We also discuss consistency of our model with various other measurements, and in particular consistency with local measurements of the Hubble parameter. We also point out possible observable signatures.

Keywords: superclusters, cosmological parameters from CMBR, dark energy theory, cosmic flows

ArXiv ePrint: [0712.0370](https://arxiv.org/abs/0712.0370)

Contents

1	Introduction	1
2	Large scale structure and LTB metrics	3
3	The Minimal Void Model	4
4	Supernovae fits	6
4.1	Analytical results	6
4.2	Numerical analysis	7
5	MCMC fit of the WMAP data	8
6	Conclusion and discussion	14
A	Analytical results for LTB metric	15
A.1	Metric & density profile	15
A.2	Photon trajectories	16
A.3	Luminosity distance vs. redshift	17
A.4	The “Jump”	18
A.5	CMB dipole moment	19
A.6	Analytic expression for the $D_L - z$ curve	20

1 Introduction

One of the most baffling problems in cosmology and fundamental physics today concerns the acceleration of the universe, as inferred from the redshifting of the type Ia supernovae. Along with this observation, the WMAP data and the large scale structure measurements can all be explained by invoking a dark fluid with negative pressure dubbed as dark energy. This has given rise to the so-called flat Λ CDM or concordance model consisting of approximately only 4% of visible matter (baryons), the rest being dark (approximately 3/4 dark energy and 1/4 dark matter). However, what is this dark energy and why its abundance should be such that it happens to be exactly in concordance with matter density today, remains very much a mystery.

Recently, a few researchers have tried to take a different point of view: what if the effect of large scale structure could account for the observed luminosity to redshift behavior of type Ia supernovae (i.e. give rise to an “apparent” acceleration of the universe), without Dark Energy? Recent studies of exact solutions to the Einstein equations have, in fact, been able to reproduce the observed luminosity to redshift relation that is usually attributed to acceleration, provided that we lived in a large region (“void”) that has less matter density than the spatial average density over the cosmological Horizon [1–3] (see [4] for a review). However, in order for the void model to be taken seriously, several key issues have to be addressed.

Firstly, the observation of small, nearly scale invariant CMB temperature fluctuations, strongly supports the principle that our universe is homogeneous and isotropic on large scales. According to our current understanding of structure formation, $\mathcal{O}(1)$ non-linearities are only expected typically at scales $\sim \mathcal{O}(10\text{Mpc}/h)$. In this case one can argue that the effect of these inhomogeneities on cosmology, which is governed by the Hubble scale $\sim 3000\text{Mpc}/h$, would be too small to be significant. However, there are reasons why one could be wary of such a conclusion.

From the theoretical point of view, the non-linear behaviour of structure formation is not a trivial issue. For instance, due to non-linear effects it is known that smaller voids can percolate to form much larger underdense structures which occupy most of the volume of the Universe (see e.g. [5], according to which such a percolation has a threshold, when the density is about 50% lower than the average), forming what is known as a “cosmic web” of superclusters and voids. Also, we note that non-standard features on the primordial power spectrum, such as a spike at a particular scale, or some non gaussianity may enhance the possibility of having larger structures and voids.

Observationally speaking, several huge nonlinear structures (notably, the Sloan Great Wall has a length of $400/h$ Mpc [6]) have been revealed through surveys like SDSS and 2dF (of course, these data are only tracing the visible matter, so their interpretation in terms of total matter is subject to a bias). It is unclear whether the presence of these large observed objects is consistent with the present understanding of structure formation. Further, there has been observational evidence for the presence of a local large underdense ($\sim 25\%$ less dense) region (that extends to ~ 200 Mpc/ h) from number counts of galaxies [7]. This represents a 4 sigma fluctuation, and would be at odds with Λ CDM. More recently, there has been a claim that the presence of the cold spot in the CMB detected in the WMAP sky [8] is also associated with a similar Big Void in the large scale-structure [9]. Intriguingly, the presence of such Big Voids has also been advocated by [10] in order to explain some features of the low multipole anomalies in the CMB data (in addition to the cold spot). Finally we note that two recent papers [11, 12] claim a significant (95% C.L.) detection of an anisotropy in the local Hubble flow in the *Hubble Key Project* data [12] and in the SN Ia dataset [11]. These would be completely natural consequences of being inside a large local void [13], since, of course, we are neither expected to be exactly at the center nor the void is not expected to be exactly spherical.

However, it is fair to say that the presence of large voids becomes more unlikely (thus requiring probably a non-conventional paradigm of structure formation), as the size of the void and the density contrast that we consider become larger. This emphasizes the need to find the “Minimal Void (MV) Model” i.e., with minimal length scale and underdensity contrast that is required to give a *consistent fit* to the supernovae data (the reader will easily recognize that the larger is the void, in general the better is the fit) . This is the first goal of our paper.

The second important issue that one has to address in the context of the MV model is whether it can reproduce the successes of Λ CDM model for many different observations, most notably the WMAP third year data. In this paper we present an analysis of the MV model subject to the WMAP 3yr data using the COSMOMC package [14], using a Monte Carlo Markov Chain (MCMC) method. Finally we combine the CMB analysis with the SN Ia data, to constrain local measurements of the Hubble parameter.

Our model consists of a matter dominated Universe (EdS) plus a Void, but actually reduces to fitting WMAP with a pure EdS Universe, since, as we will show, the corrections induced by a Void of $200 - 300\text{Mpc}/h$ radius for a central observer are negligible for CMB observations. A similar analysis has already been done in EdS by [15–17]; nonetheless,

for completeness of the presentation and to better combine the constraints from CMB and supernovae, we perform an independent analysis of the WMAP 3 yr data. We obtain results similar to [15, 16], although we use different priors on the primordial spectrum, lending robustness to the findings of [15, 16]. We show how it is possible to *combine* WMAP and SN data in the Void model, and how this leads to higher values of the local Hubble parameter in the Void model with respect to the pure EdS model.

As an aside we note that we obtain analytical expressions for the luminosity-redshift curve for arbitrary density profiles which are excellent approximations even when the local inhomogeneous patch extends up to $\sim 400 \text{ Mpc}/h$.

We now proceed as follows: in section 2, we introduce our swiss-cheese model and briefly discuss the non-linear structure formation, as well as the photon propagation in this configuration. In section 3 we explain qualitatively how the MV model can be consistent with both the supernovae and WMAP data, as well as local measurements of the Hubble parameter. In section 4, we perform supernovae fits for the void model. Next in section 5, we perform a MCMC analysis of the WMAP data without a cosmological constant. Finally, we conclude by summarizing our findings, suggesting possible future directions, and also pointing out unique predictions of the MV model. The appendix contains approximate analytical solution of the trajectory, redshift and luminosity distance of a photon in the radially inhomogeneous “LTB” (Lemaitre-Tolman-Biondi) metric.

2 Large scale structure and LTB metrics

As emphasized in the introduction, in this paper we will advocate that perhaps we are sitting near the centre of a “Big Void” spanning a radius of $\sim 200 \text{ Mpc}/h$ which, as we will explain, is roughly the minimal size needed to account for the SN-Ia supernova data (although one can go down to values of about $150 \text{ Mpc}/h$ by accepting a slightly worse fit).

To accurately model such inhomogeneous structures/voids we use the spherically symmetric LTB metric [18], which describes “radially” inhomogeneous patches of any desired radius, L (such metric describes the most generic spherically symmetric dust-filled space-time; we refer to appendix A for definitions and details). Such spherical patches can be pasted onto a homogeneous FLRW metric consistently [19], which also ensures that the average density inside the spherical patch is the same (almost exactly, see again appendix A for details) as the background density outside the patch. Thus, an underdensity around the central region is compensated by a shell-like structure near the circumference.¹

Technically, it is somewhat complicated to describe the dynamics of the LTB metric (see appendix A for details and for the choice we made for the so-called mass function), but intuitively it is as if one had an independent scale factor corresponding to each (comoving) radial coordinate, r , which is evolving as an independent FLRW metric with a given spatial curvature $k(r)$. *A priori*, $k(r)$ is an arbitrary function which also determines the density profile. Assuming $L \ll R_H$ (the Hubble radius) one has

$$\rho(r, t) \simeq \frac{\langle \rho \rangle(t)}{1 + (t/t_0)^{2/3} \epsilon(r)}, \quad \text{where } \langle \rho \rangle(t) \equiv \frac{M_p^2}{6\pi t^2}, \quad \text{and } \epsilon(r) \equiv 3k(r) + rk'(r). \quad (2.1)$$

We observe that the FLRW behaviour for the density is given by the factor $\langle \rho \rangle(t)$, while the fluctuations are provided by the presence of $\epsilon(r)$ in the denominator. When $\epsilon(r)$ is close

¹In fact we may speculate that the Sloan Great Wall may be indicative of such a shell-like structure, given its location, at about $250 \text{ Mpc}/h$ away from us, and its two-dimensional shape [6].

to its maximum value we have a void, while when it is close to its minimum, it signals an overdensity. Note that at early times the density contrast $\delta(r, t) \equiv (\rho(r, t) - \langle \rho \rangle(t)) / \langle \rho \rangle(t)$, defined in the usual way, grows as $t^{2/3}$, in agreement with the prediction of cosmological perturbation theory. On the other hand at late times, when $(t/t_0)^{2/3} \epsilon(r) \sim \mathcal{O}(1)$, the density contrast grows rapidly (and this result is the same as found within the Zeldovich approximation [20]). In fact, for an overdense region, the structure ultimately collapses, as to be expected because LTB metrics cannot account for virialization that we observe in nature. Nevertheless, for our purpose, as long as we do not reach the collapse time, LTB metrics adequately capture the effects of non-linear structure formation on photon propagation.

Now, we are interested in modeling a spherical void region surrounded by a compensating shell-like structure, and this is obtained using a $k(r)$ which starts off from a maximum at $r = 0$ and falls off to a constant value at $r = L$ such that

$$k'(0) = k'(L) = 0, \quad (2.2)$$

$$k(L) = \frac{4\pi}{3} \Omega_k, \quad \text{for } |\Omega_k| \ll 1, \quad (2.3)$$

One can check that such an LTB metric can consistently match to an FLRW background [19], with curvature abundance Ω_k . In this paper we will mostly focus on a background FLRW metric which is flat. The essential reason for choosing a flat background metric is that curvature is known to be constrained to be very small in order to get a good fit of the WMAP data along with other measurements (such as measurements of the Hubble constant [21]). We note in passing that in LTB models we are considering we do not have back-reaction effects in the outside region, i.e. on the average the FLRW regions do not feel at all the presence of holes. The particular choice of the curvature function that we employ to model the inhomogeneities and fit the supernova data is given by

$$k(r) = k_{\max} \left[1 - \left(\frac{r}{L} \right)^4 \right]^2. \quad (2.4)$$

One can check that eq. (2.4) satisfies eq. (2.3), in the case with $\Omega_k = 0$. It contains two important physical parameters, L and k_{\max} , which correspond to the length-scale and amplitude of fluctuations respectively.²

3 The Minimal Void Model

As we shall see later, we need to invoke a Big Void with a radius of about $200/h$ Mpc (and with average density contrast of roughly $\langle \delta^2 \rangle \simeq 0.4$). The probability of having non-linear structures at larger scales becomes progressively smaller. Using the conventional *linear* and *Gaussian* power spectrum for radii of about ~ 200 Mpc/ h the typical density contrast is only of about 0.03 – 0.05 (for a radius of ~ 160 Mpc/ h the typical contrast is instead about 0.06).

So, as stated in the Introduction, we would like to find the “Minimal Void Model” i.e., with minimal length scale and underdensity contrast that is required to give a consistent fit to

²The exponent of r/L has been chosen to be equal to 4, but the reader may note that any exponent $n > 1$ is good, as well. Varying n one varies the width of the shell-like structure. The larger the n , the flatter the void, and narrower the structure. However, we choose to stick only to the case $n = 4$, since it already gives us a sufficiently flat profile for the underdense region which we found to improve the supernova fit, and anyhow the whole analysis and discussion is not very much affected by the precise shape of the shell.

the supernova data. This is obtained by realizing that the crucial evidence for acceleration comes from the fact that we observe a mismatch between the expansion at low redshifts (between roughly $0.03 \leq z \leq 0.07$) and the expansion at higher redshifts (where supernovae are observed [22], between roughly $0.4 \leq z \leq 1$). This situation arises because of the current experimental status of supernovae observations: we have very few data in the redshift range between 0.07 and 0.4. The situation will dramatically change with the coming release of the SDSS-II supernovae data [23], which will include about 120 data points in upcoming first year data release, ranging between redshifts 0.05 and 0.4.³ Thus it is not necessary to alter the EdS $D_L(z)$ all the way up to $z \sim \mathcal{O}(1)$, but a large correction to the Hubble expansion in the local region, $0.03 \leq z \leq 0.07$, stretching up to $\sim 200 \text{ Mpc}/h$, may be sufficient. In particular if we are living in a local underdensity, then we experience extra stretching as voids become “more void” (that is how structure formation works) which manifests as a local Hubble expansion rate larger than average (outside the patch), precisely what is required to mimic acceleration. Another way of seeing this is that all sources in the local region have a collective radial peculiar velocity due to the gravitational attraction of the shell-like structure, which adds to the overall expansion.

Let us now see more precisely how the MV model works. We first focus on the high redshift region, i.e. outside the LTB patch. In this region the $D_L(z)$ curve of the MV model basically corresponds to that of the homogeneous EdS curve parameterized by a lower average Hubble parameter,⁴ h_{out} . Further, in this range of high redshift supernovae, the EdS curve can run very close to the ΛCDM model, albeit with a different, slightly lower, Hubble parameter, h_{out} as compared to the Hubble parameter h of the ΛCDM curve. For instance, if we compare the EdS distance (D_E) with the ΛCDM distance (D_Λ) [27]:

$$\frac{D_E}{D_\Lambda} \equiv \mathcal{R}(z), \quad (3.1)$$

it turns out that the ratio \mathcal{R} does not change much in the relevant range of high- z supernovae, $0.4 \leq z \leq 1$:

$$\mathcal{R}(0.4)/\mathcal{R}(1) \simeq 1.12. \quad (3.2)$$

Moreover, the ratio $\mathcal{R}(z)$ itself is proportional to the ratio h/h_{out} . Thus, by choosing the latter ratio appropriately, the luminosity distance of the average EdS model can be made to approximately coincide with that of the ΛCDM one in the redshift range $0.4 \leq z \leq 1$.

Next, let us look at the low redshift region. In this region, the $D_L(z)$ curve is basically linear, the slope being given by the Hubble parameter:

$$H_0^{-1} \equiv \lim_{z \rightarrow 0} \frac{D_L(z)}{z} = \frac{3000 \text{ Mpc}}{h}. \quad (3.3)$$

³We can estimate the impact on the χ^2 simulating 120 points [23] randomly distributed in this range, assuming a concordance ΛCDM reference model and assuming an error in magnitudes of Δm . The difference in χ^2 for our best fit MV model would be of order $\Delta\chi^2 \sim 70$ for $\Delta m = 0.15$ (which is the typical intrinsic dispersion used in SNIa analysis). Therefore such data can be used to discriminate between our model and concordance ΛCDM .

⁴We may briefly discuss the difference between LTB and EdS models in the outer region as follows. First of all, there is an integrated effect (Rees-Sciama), which goes like $(L/r_H)^3$, leading to an $\sim \mathcal{O}(10^{-5})$ effect [24]. There is also a shift due a local effect (the Sachs-Wolfe effect), since the value of the gravitational potential at the centre differs from the one of the outer sources by an amount of order $(L/r_H)^2$. Both effects for $\mathcal{O}(300)\text{Mpc}/h$ sized Voids lead only to a small shift in the CMB monopole, which can safely be neglected. Finally, as stressed in [24–26] there are in general $(L/r_H)^2$ corrections to the luminosity distance in the LTB metrics due to Lensing effects, but these effects are actually zero when averaged over the entire sky, or when the observer is at the centre.

Thus in order for the MV model to agree with the best-fit Λ CDM, the Hubble parameter inside the LTB patch should coincide with the measured local Hubble parameter.

As we will see later, we find a very good fit to the SN data (where we use the dataset [22]), with goodness-of-fit $\sim 50\%$, without Λ in the MV models. Assuming our model, a parameter estimation (with likelihood $e^{-\chi^2/2}$) gives at 95% C.L. the following range for the jump parameter:

$$1.17 \leq \mathcal{J} \equiv \frac{h}{h_{\text{out}}} \leq 1.25. \quad (3.4)$$

On the other hand the fit to the WMAP data will fix the value of the global h_{out} . As we will see in section 5, this is the important quantity for the photons that come from the last scattering surface, and not for example the local h . Crucially, a reasonable fit of the WMAP data without Λ requires a relatively low Hubble parameter outside the Void:

$$0.44 \leq h_{\text{out}} \leq 0.47, \quad (3.5)$$

(at 95% C.L.).

Now, these two constraints (h_{out} from CMB and the \mathcal{J} from Supernovae) can be combined together leading to

$$0.51 \leq h \leq 0.59. \quad (3.6)$$

(see figure 5) and we have to compare this with the local measurements.

These local values typically vary over a wide range. The Hubble parameter measured using supernovae [28] reads $h = 0.59_{-0.04}^{+0.04}$, the Hubble Key Project [21] measures a value of $h = 0.72_{-0.08}^{+0.08}$ (although in [29] a lower value of $h = 0.62_{-0.05}^{+0.05}$ is given, with an improved treatment of Cepheids). Measurements of clusters using Sunyaev-Zeldovich distances [30] (which is based on data at different redshifts, up to $z \simeq 1$) gives a much lower estimate, $h = 0.54_{-0.03}^{+0.04}$ (in EdS), although a more recent revision of the data [31] leads to higher values, consistent with HST. Also, measurements at high redshift ($0.3 < z < 0.7$) using gravitational lensing [32] give $h = 0.48_{-0.03}^{+0.03}$ (for a more comprehensive summary see [16]). In fact, the value of h estimated also seem to decrease as one looks at sources with larger redshifts which would be a prediction for the MV model.

For reference, a range to consider for h , would be perhaps:

$$0.55 \lesssim h \lesssim 0.8. \quad (3.7)$$

This can now be used also to pinpoint the underdensity contrast required in the void. As we will analytically show in the next section (and verify numerically), the jump parameter in LTB models does not depend on the details of the curvature (density) profile, but only on the amplitude k_{max} , or equivalently the maximal underdensity contrast at the center of the void. We find that a central underdensity between 44% and 58% reproduces the relevant range eq. (3.4) of the jump parameter, and it is easy to check that this is also consistent with eq. (3.7) and eq. (3.5). Notice however that the average underdensity is always somewhat smaller than the central value, see e.g. figure 2.

4 Supernovae fits

4.1 Analytical results

Our aim in this section is to quantitatively fit the supernova data (we use here the dataset from [22]) using the MV model. In order to have better control, we decided to perform both

numerical and analytical analysis. As explained in [24], as long as $L \ll R_H$, one can find excellent approximations to the luminosity distance-redshift relation. In the appendix we have obtained expressions for $D_L(r)$ and $z(r)$ (which can be used to obtain $D_L(z)$ implicitly) for any general profile. We also provide the reader with a summary of all the equations necessary to reproduce the analytic approximation for $D_L(z)$ in appendix A.6, in a self-contained form. Inside the LTB patch, the redshift as a function of the radial coordinate looks like

$$z \approx \frac{2r}{3t_0} [1 + 2f(3k(r)/\pi)] . \quad (4.1)$$

while the angular distance is simply given by

$$D_A = r [1 + f(3k(r)/\pi)] . \quad (4.2)$$

In deriving these formulas we have used a specific choice of the radial coordinate, given in eq. (A.37) of appendix A.6, such that r approximately corresponds to the proper distance today.

The luminosity distance, in General Relativity, is always related to the angular diameter distance [33] D_A via

$$D_L = (1 + z)^2 D_A . \quad (4.3)$$

One can easily verify that, in the above expressions for D_A and z , the terms outside the brackets correspond to the FLRW results for a flat universe. f is an universal function (it does not depend on the profile) defined in the appendix, which gives us the deviation of the $D_L(z)$ curve from the FLRW result. As one can see, our analytical results agree very well with the numerical solutions, see figure 6.

Now, one defines the Hubble parameter as the initial ($z=0$) slope in the $D_L - z$ plot: using this definition one can obtain (see appendix A.4 for details) an exact relation between the jump parameter and the central density contrast:

$$\mathcal{J} = \frac{h}{h_{\text{out}}} = 2 - (1 - |\delta_0|)^{1/3} . \quad (4.4)$$

Surprisingly, this expression does not depend on the specific form of the profile, and therefore lends generality to the analysis.

4.2 Numerical analysis

We employ in this section a two steps strategy. First, without even using the LTB metric, we try to fit the data with a crude approximation of the void, which consists of an empty (curvature dominated) FLRW Hubble diagram for the inner region and then an EdS Hubble Diagram for the outer region. Between the two regions ($z < z_{\text{jump}}$ and $z > z_{\text{jump}}$) there is a discontinuous jump in the Hubble parameter $H_{\text{in}}/H_{\text{out}}$. In this way we get a good idea about what are the best values for \mathcal{J} and z_{jump} . The results are shown in the left plot of figure 1.

As one can see from the plot, the larger is the value for z_{jump} the better is the fit. However, we do not gain much by taking z_{jump} larger than, say, 0.08 (which corresponds to a radius of 250 Mpc/h). It is also interesting to note that a z_{jump} as low as 0.05 (which corresponds to a radius of 150 Mpc/h) still gives a reasonable fit (goodness-of-fit is higher than a few %). Almost independent of z_{jump} , the best value for the jump is around $\mathcal{J} \simeq 1.2$.

As a second step, we try to reproduce these results with a full LTB study. For simplicity we focus on only one value of L for the LTB patch ($z_{\text{jump}} \approx 0.085$). A further observational

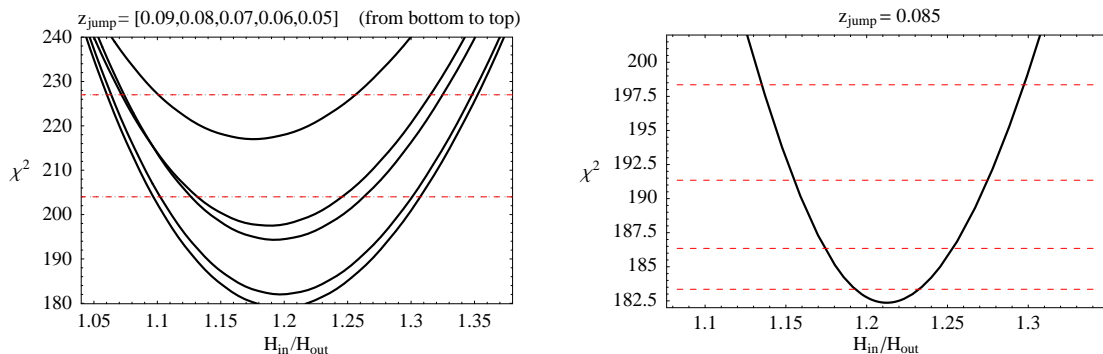


Figure 1. The χ^2 for Supernovae IA as a function of the jump $h/h_{\text{out}} = H_{\text{in}}/H_{\text{out}}$, for different values of the size of the inhomogeneous region (whose boundary ends at redshift z_{jump}). We have used in the left plot a model with two FLRW regions (empty inside and EdS outside), with two different Hubble parameters. From bottom to top the solid curves correspond to $z_{\text{jump}} = [0.09, 0.08, 0.07, 0.06, 0.05]$. The two dashed lines correspond to a 10% and a 1% goodness-of-fit. In a full specific LTB model, matched to FLRW at redshift $z_{\text{jump}} = 0.085$. In the right plot we use a full LTB model, matched to FLRW at redshift $z_{\text{jump}} = 0.085$. The dashed lines correspond to the 1σ , 2σ , 3σ and 4σ where we used as a likelihood $e^{-\chi^2/2}$. The number of d.o.f. is 181 (we have used the Riess Gold dataset [22]).

motivation for considering such a redshift comes from the fact that it also approximately coincides with the redshift of the Sloan Great Wall, which spans hundreds of Mpc across and it could be suggestive of being the “compensating structure” expected at the boundary of the LTB patch [6]. In the profile eq. (2.4), we therefore fix the radius L , and let k_{max} vary (which corresponds to varying the jump \mathcal{J} , or equivalently the central density contrast δ_0). We find that the 1σ range of the jump corresponds to $1.214_{-0.019}^{+0.019}$ (see right plot of figure 1). For the density contrast at the center this translates to $\delta_0 = 0.514_{-0.036}^{+0.034}$.

Let us comment briefly on the values that we get for the χ^2 as compared to other models. The EdS model has a very bad fit to the data. On the other hand the Λ CDM model has a much lower χ^2 than our model ([22] quotes 150),⁵ which is indeed strangely too low.⁶ Now, in terms of goodness-of-fit our χ^2 is what one expects typically, since it is roughly equal to the number of d.o.f., and this makes our model a good fit to the data.

Note that we have fitted only to the “Gold” dataset [22], although there are more up-to-date ones since our purpose is just to check the consistency of the model.

Finally we show, as an illustration, one example of a plot of $D_L - z$ in figure 2 together with the shape of the density profile (as a function of z).

5 MCMC fit of the WMAP data

It is commonly assumed that the Λ CDM model, with a non-zero cosmological constant, is the only one which can adequately explain the CMB spectrum. This is based on the result that

⁵The open empty Universe has also a low χ^2 , of about 160.

⁶We note here that all the SN fits are plagued by not knowing exactly what are the errors on the SN measurements. In fact, if one used only instrumental errors, then the data points would have a very large scatter with tiny errors, and there is no smooth curve which can give a fit to the data. Then what is done by SN collaborations is to add an error of about 0.15 magnitudes due to the intrinsic variability. Introducing such an error is what makes the concordance Λ CDM χ^2 so low (see e.g. table 7 of [34], where the error due to the intrinsic variability is determined by requiring that $\chi^2/d.o.f. = 1$ for the nearby supernovae).

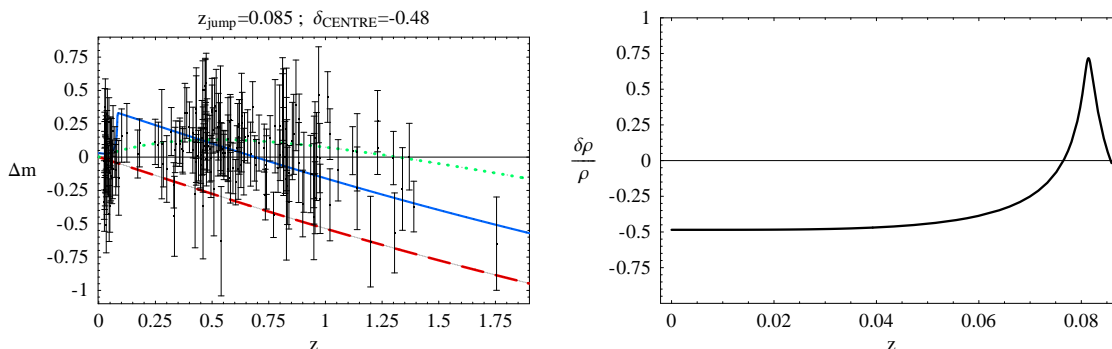


Figure 2. In the left plot we show a fit of the Supernovae data (Riess et al. [22]) with an LTB model which has $\chi^2 = 186$ (the d.o.f. are 181). The inhomogeneous patch extends up to $z \simeq 0.085$ and the underdensity in the center is $\delta_{\text{CENTRE}} = -0.48$. We have shown $\Delta m \equiv m - m_{\text{empty}}$: the magnitude ($m \equiv 5 \text{Log}_{10} D_L$) minus the magnitude of an empty open FLRW Universe as a function of the redshift z . The blue solid line is our inhomogeneous model, the red dashed-line is an EdS model (whose Hubble constant is normalized through the nearby supernovae), the green dotted line is the best-fit Λ CDM. In the right plot we show the density contrast for the same model, as a function of z . The average contrast ($\sqrt{\langle \delta^2 \rangle}$) in the inhomogeneous patch is 0.43 ($\sqrt{\langle \delta^2 \rangle} \simeq 0.33$ in the underdensity, $\sqrt{\langle \delta^2 \rangle} \simeq 0.48$ in the overdensity).

once one assumes a “flat” prior on Λ , it turns out that the “most likely” parameters, given the WMAP data, correspond to $\Omega_\Lambda \sim 0.7$. The question that we want to ask however, is about consistency of WMAP with EdS: can we get a reasonable fit to the CMB spectrum even after setting Λ to zero? To put it differently, if we had a strong theoretical prejudice against having a non-zero cosmological constant, or if there were other observations disfavoring it, then would the 3-yr WMAP data independently rule out an $\Omega_M = 1$, EdS universe? (Here M means total matter = baryons + dark matter).

Rigorously speaking, fitting the CMB in our model seems technically challenging because one would have to compute the secondary effects, i.e. what the spectrum of the CMB radiation would look like after passing through the local underdense region (and maybe many other such regions),⁷ it encounters on its journey to us. According to [24], the corrections to the redshifts of photons which pass through a void of size L is a Rees-Sciama effect that goes like $(L/R_H)^3$. A coherent addition of this effect due to many voids could produce a correction of order $(L/R_H)^2$. Thus for a void with a typical radius $\sim 200/h$ Mpc that we considered in this paper, such a cumulative effect could be $\sim 10^{-2} - 10^{-3}$. This can be ignored for the study of supernovae. If these many voids exist, they would give a sizable effect on the CMB. The number $\sim 10^{-2} - 10^{-3}$ would refer to a monopole in the CMB, while the correction to higher multipoles would be smaller (depending on how different is the number of voids along different directions in the sky). However, in this paper we ignore such secondary effects. On the qualitative side, we expect this to be important only for small l and decay fast for larger l , and it should act in the same way as an Integrated Sachs-Wolfe effect.⁸

⁷The assumption that we live in a void could naturally lead us to consider that the universe might contain many such voids, a bubbly universe. In this case one would have to compute the passage of the photons through many such voids.

⁸Let us note that in a EdS Universe it would be impossible to fit the claimed detections of ISW correlations [36], since this is exactly zero at the linear level. Having Voids instead can allow the existence of a larger effect, which in principle could be tested against such observations, although this goes beyond the scope of

	Λ CDM		EdS $\alpha_s = 0$		EdS $\alpha_s \neq 0$		Curved $\alpha_s, \Omega_k \neq 0$	
	<i>min</i>	<i>max</i>	<i>min</i>	<i>max</i>	<i>min</i>	<i>max</i>	<i>min</i>	<i>max</i>
$\Omega_b h_{\text{out}}^2$	0.005	0.04	0.005	0.04	0.005	0.04	0.005	0.04
$\Omega_m h_{\text{out}}^2$	0.01	0.3	0.01	0.3	0.01	0.3	0.01	0.3
Ω_Λ	0	1	0	0	0	0	0	0
n_s	0.5	1.5	0.5	1.5	0.5	1.5	0.5	1.5
α_s	0	0	0	0	-0.3	0.3	-0.3	0.3
Ω_k	0	0	0	0	0	0	0.05	0.05
z_{re}	4	20	4	20	4	20	4	20
$10^{10} A_s$	10	100	10	100	10	100	10	100

Table 1. Priors for different parameters in the COSMOMC Runs. Here $\Omega_b h_{\text{out}}^2$ is the physical baryon density, $\Omega_m h_{\text{out}}^2$ is the physical dark matter density, z_{re} is the redshift at re-ionization, n_s is the spectral index, α_s is the running of the spectral index and A_s is the amplitude of scalar fluctuations (for definitions see, e.g. [14]).

The correction to the CMB redshift that comes from our local void, instead, will depend on how symmetric the void is, and how “centrally” we are located. For an off-center observer, in appendix A.5 we perform a non-perturbative estimate of the dipole moment, and find that in order for it to not exceed the observed value $\sim \mathcal{O}(10^{-3})$, “we” must be located very close to the center, approximately within 10% of the void-radius, in concordance with the findings in [35]. In this case the correction to the higher multipoles are much more suppressed and not visible in CMB [35]. Departure from spherical symmetry, on the other hand, may have a much more interesting effect, specially on the lowest l s in the CMB spectrum, and could be visible.⁹

As stressed in the introduction, an analysis of the CMB has been already done in EdS by [15, 16]. However, we have done an independent analysis again in the present paper to have a complete presentation of how the constraints from the WMAP and SN data sets can be combined, and in particular its implications for the Hubble parameter. An additional difference is that we consider a spectrum with nonzero spectral index and running, while in [15, 16] the authors assumed different priors (such as different power law indices, or the existence of a bump and a change in the amplitude in the primordial spectrum), rather than considering an overall running.

As one would expect, we find that if one assumes as priors, no dark energy, as well as no additional features in the primordial spectrum (other than spectral index and amplitude) the fit of the 3-yr WMAP data is very poor. However the situation changes if we introduce a “running in the spectral tilt”, α_s , in the observable ~ 7 e-folds of our universe in CMB (following the same definition as in [14])(see table 4).

We have performed a Monte Carlo Markov Chain (MCMC) analysis of the WMAP 3 year data using the program COSMOMC [14], with the priors given in table 1. We used the version of the COSMOMC program which lets one analyze the range $2 \leq l \leq 30$ for TT correlations and the range $2 \leq l \leq 23$ for TE+EE correlations using the pixel-based approach (T, Q and U maps), which offers a much more accurate treatment of the low- l likelihood [45]. One has (957+1172) pixel data in all. The rest of the correlations that we

the present work.

⁹In this context we note that similar effects in anisotropic geometric void configurations have been used to explain the low multipole anomalies in the CMB sky [10].

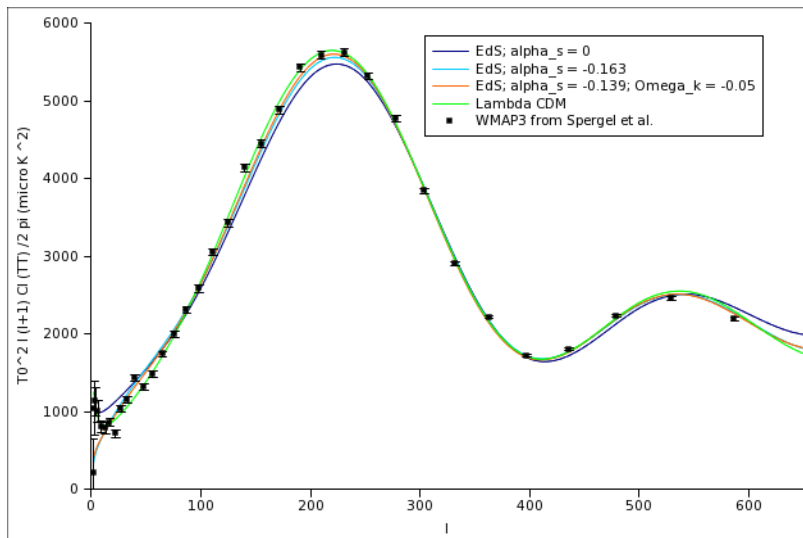


Figure 3. Λ CDM and EdS fits to the WMAP 3 binned data.

	Λ CDM	EdS, $\alpha_s = 0$	Eds, $\alpha_s \neq 0$	Eds, $\alpha_s, \Omega_k \neq 0$
$\Omega_b h_{\text{out}}^2$	$0.022^{+0.002}_{-0.002}$	$0.022^{+0.001}_{-0.001}$	$0.018^{+0.001}_{-0.002}$	$0.019^{+0.002}_{-0.001}$
$\Omega_m h_{\text{out}}^2$	$0.106^{+0.021}_{-0.013}$	$0.198^{+0.008}_{-0.011}$	$0.186^{+0.011}_{-0.009}$	$0.167^{+0.009}_{-0.007}$
Ω_Λ	$0.759^{+0.041}_{-0.103}$	0	0	0
z_{re}	$11.734^{+4.993}_{-7.619}$	$8.697^{+4.351}_{-6.694}$	$13.754^{+2.246}_{-5.752}$	$13.342^{+2.55}_{-5.011}$
Ω_k	0	0	0	0.05
n_s	$0.96^{+0.04}_{-0.04}$	$0.94^{+0.021}_{-0.038}$	$0.732^{+0.07}_{-0.071}$	$0.761^{+0.069}_{-0.069}$
α_s	0	0	$-0.161^{+0.044}_{-0.044}$	$-0.13^{+0.037}_{-0.048}$
$10^{10} A_s$	$20.841^{+3.116}_{-3.442}$	$25.459^{+2.135}_{-2.766}$	$25.302^{+2.182}_{-2.968}$	$23.975^{+2.198}_{-2.448}$
Ω_m/Ω_b	$4.73^{+0.999}_{-0.485}$	$9.119^{+0.341}_{-0.357}$	$10.094^{+0.645}_{-0.489}$	$8.929^{+0.512}_{-0.541}$
h_{out}	$.72857^{+0.05137}_{-0.07393}$	$.46857^{+0.00888}_{-0.01307}$	$.4523^{+0.01291}_{-0.01129}$	$.42069^{+0.01107}_{-0.00919}$
Age/GYr	$13.733^{+0.389}_{-0.369}$	$13.908^{+0.399}_{-0.258}$	$14.408^{+0.369}_{-0.4}$	$15.338^{+0.342}_{-0.393}$
σ_8	$0.77^{+0.121}_{-0.109}$	$1.012^{+0.056}_{-0.081}$	$0.919^{+0.07}_{-0.075}$	$0.862^{+0.06}_{-0.063}$
τ	$0.095^{+0.072}_{-0.074}$	$0.047^{+0.037}_{-0.041}$	$0.079^{+0.023}_{-0.044}$	$0.081^{+0.024}_{-0.041}$

Table 2. Most likely parameter values with 1σ errors for the various COSMOMC Runs.

considered consisted of C_l^{TT} in the range $31 \leq l \leq 1000$, and C_l^{TE} in the range $24 \leq l \leq 450$.

We find that an EdS universe with *no dark energy* but with a value of the Hubble constant, H_{out} , significantly lower than the conventionally accepted value of 70 km/s/Mpc gives a very reasonable fit to the CMB spectrum, see figure 3 and table 4. The most likely parameter set along with their 1σ bounds are tabulated in table 2.

We also produce two 2-dimensional likelihood contour plots: (i) h_{out} vs. Ω_m/Ω_b which are the only two independent parameters related to the composition of the universe, and (ii) n_s vs. α_s which characterize the spectrum.

In figure 5 we show a contour plot combining the constraint from supernova fit in the previous section with that of WMAP. As promised before, we find that the locally measured

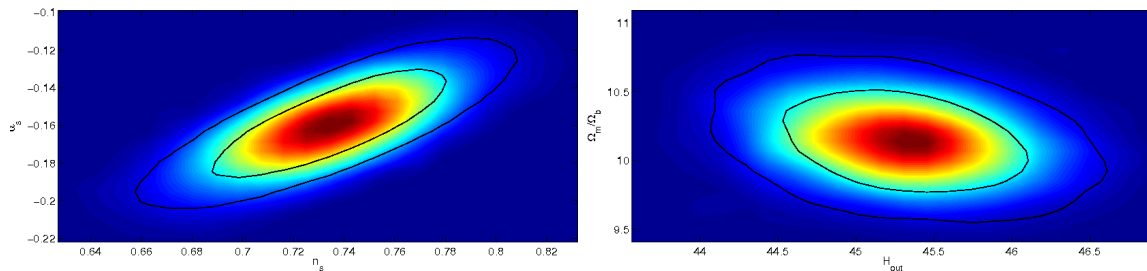


Figure 4. Contour marginalized likelihood plots to the WMAP 3-yr data for the run “EdS, $\alpha_s \neq 0$ ”. The coloured map corresponds to mean likelihood, while the solid lines correspond to marginalized 1- σ and 2- σ contours.

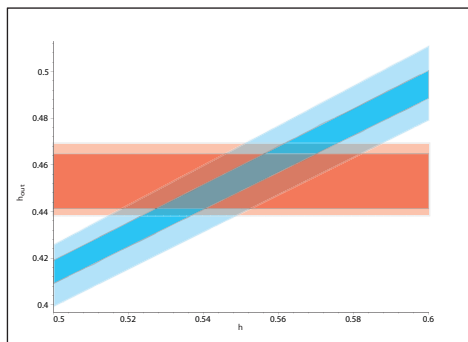


Figure 5. 1- σ and 2- σ Contour plots for h vs. h_{out} . The blue bands come from the SN-I analysis, while the red bands correspond to constraints coming from WMAP.

Hubble parameter can be as high as $h \sim .59$ at the 2σ , or 95% C.L., which is within the acceptable range of the different measurements of the Hubble parameter.

Let us briefly discuss about the values that we obtain for the other cosmological parameters.

The main constraint on the baryon density comes from BBN [37], $0.017 \leq \Omega_b h_{\text{out}}^2 \leq 0.024$ at 95% C.L. This is indeed consistent with the parameter range that we obtain from the WMAP run, $\Omega_b h_{\text{out}}^2 = 0.018_{-0.002}^{+0.002}$. Although we have a higher baryonic abundance, the lower Hubble parameter almost precisely compensates to yield approximately the same baryonic energy density as it is obtained in the “concordance” Λ CDM model, as already noted in [16]. As one can see from the likelihood plot, figure 4 as well as table 2, the ratio between dark matter and baryons is somewhat higher, $\Omega_m/\Omega_b \sim 10$, than the “concordance” Λ CDM model value of $\Omega_m/\Omega_b \sim 6$.

Then, our best fit spectral index is relatively low, $n_s \sim .73$, but there are several inflationary scenarios where such low spectral tilts are common (for example in modifications of the old inflationary scenario from false vacuum [38], or inflation from exponential potentials naturally occurring in string theories, see for instance [39]). Our model also requires a significant running, $\alpha_s \sim -.16$. We have not confronted our model with a host of other observations coming from large scale structure and weak lensing experiments, which may require refining or adding new ingredients to the model (see for instance [15, 16] for progress in these directions). For instance, it is well known that EdS based models fail to reproduce the BAO peak [15, 40, 41]. At first sight the value for $\sigma_8 = 0.92_{-0.08}^{+0.07}$, in our model also

Parameter	L	$\Omega_b h_{\text{out}}^2$	$\Omega_m h_{\text{out}}^2$	z_{re}	σ_8	n_s	α_s	δ_0	h_{out}	h
Best-fit	$250/h$	$0.018_{-0.002}^{+0.002}$	$0.19_{-0.01}^{+0.01}$	$13.8_{-5.8}^{+2.2}$	$0.92_{-0.08}^{+0.07}$	$0.73_{-0.07}^{+0.07}$	$-0.16_{-0.04}^{+0.05}$	$0.51_{-0.04}^{+0.03}$	$0.452_{-0.011}^{+0.013}$	$0.55_{-0.023}^{+0.024}$
Acceptable-fit	$160/h$	0.02	0.2	13.8	0.92	0.73	-0.16	0.44	0.47	0.55

Table 3. Best-fit Minimal Void Model Parameters.

seems too high, which may be inconsistent with measurements of the Lyman- α forest [42]. Finally, we may not also be able to fit the turnaround point of the galaxy power spectrum, which is mostly controlled by the product $\Omega_m h$, and as compared to the standard value of $\Omega_m h \approx 0.21$, this is too high in our model, although the analysis of [15, 16] shows that the addition of a hot component (neutrinos) helps to fit the galaxy power spectrum (SDSS data main sample). Ideally however, one should revisit these analysis in the light of MV model that we have presented, by including running of the tilt as well as the non-standard $D_L(z)$ relation in these inhomogeneous models,¹⁰ an important task that we leave for future. In any case, the main aim of our paper is to demonstrate, that one can be consistent with CMB, supernovae, BBN and local measurements of the Hubble parameter once one is willing to give up the cosmological principle.

Finally, we note that our value of the re-ionization epoch (optical depth) is broadly consistent with the usual observations [44] (see also discussion in [45]).

To summarize, our best fit (WMAP + SNIa) MV model consists of 8 parameters, one of which, the length scale of the void, has been chosen at the value $L = 250/h$ to derive our best-fit model. However, as noted in the introduction, if one “accepts” a G.F. $\sim 10\%$ to the supernovae data, then one can go down to a much smaller length scale, $L \sim 160/h$. Out of the other seven parameters, six of them (columns 2 to 7 in the table of 3 are obtained from the fit to the WMAP 3-yr data using COSMOMC, while the last one, (column 8), is constrained from the supernovae data. We note that a “minimally acceptable” model with respect to the central underdensity contrast would be obtained with a maximally acceptable $h_{\text{out}} \sim 0.47$, at the 95% C.L.. This in conjunction with eq. (3.7), then tells us that the minimal jump parameter has to be 1.17, or equivalently $\delta_0 \sim 0.44$. Using these information we tabulate all the parameters in table 3 for our “best-fit” and “minimally-acceptable” model. We note that the values of δ_0 and L in the “minimally-acceptable” fit is not far from what observationally is suggested in [7].

We should clarify that although we quote comparative statistics between MV and Λ CDM model, it is only meant as a guide, our aim here is not to compete with the Λ CDM model. According to the Bayesian statistical likelihood analysis of both the supernovae and the CMB data, our best fit MV model is still disfavored by many standard deviations as compared to the concordant Λ CDM model. Crucially however, such an inference is based on assuming a “flat” prior on the value of the cosmological constant. In other words it relies on the a priori assumption that all the values of the cosmological constant are equally likely. According to the Bayesian theory, such a priori probabilities are to be assigned based on theoretical prejudice. In other words, if we had a different theoretical prejudice (for example that a non-zero cosmological constant is “unphysical”), then we could just ask the question whether a non-homogenous matter distribution can fit the data, with an acceptable value of the goodness-of-fit.

¹⁰For some of these measurements we would also need to understand the growth of density fluctuations in an LTB metric, a problem which has only been recently attacked in [43].

Model	C_l^{TT}		$C_l^{TT} + C_l^{TE}$		Total	
	χ_{eff}^2	G.F.	χ_{eff}^2	G.F.	χ_{eff}^2	G.F.
Concordant Λ CDM	1038.9	4.7%	1455.2	11.3%	3538.6	41%
EdS $\alpha_s = 0$	1124.6	0%	1711.9	0%	3652.3	6%
EdS $\alpha_s \neq 0$	1057.8	1.9 %	1475.5	5.7%	3577.4	24.6%
EdS $\alpha_s, \Omega_k \neq 0$	1048.7	2.9%	1466	7.9%	3560.9	31.1%

Table 4. χ_{eff}^2 and goodness-of-fit for the different COSMOMC Runs. The first column corresponds to high- l TT power spectrum, ($31 \leq l \leq 1000$). The second column corresponds to both the high- l TT ($31 \leq l \leq 1000$) and TE ($24 \leq l \leq 450$) data. Finally, the last column contains the total statistics of TT ($2 \leq l \leq 1000$) and TE ($2 \leq l \leq 450$) spectrum.

6 Conclusion and discussion

The Type Ia supernovae data reveal that our universe is accelerating at redshifts that approximately correspond to the epoch of non-linear structure formation on large scales (the epoch of the formation of the so-called “cosmic web”). We have explored the possibility that the effect of a large scale void can account for the currently observed acceleration due to a jump between the local and the average Hubble parameter, instead of invoking a spatially constant dark energy/cosmological constant component. We find that the Minimal Void (MV) model can consistently account for the combination of the Type Ia supernovae, WMAP 3rd year, BBN constraints, provided that the void spans a radius of about of 200 Mpc/ h with a relative under density of 45%, near the center. Moreover, having a local void ameliorates the discrepancy between the low global Hubble parameter required by EdS models to fit CMB, with the local measurements of the Hubble parameter. According to our analysis at the 95% C.L. the local Hubble parameter can be as high as $h \sim .57$, which is definitely within the acceptable range eq. (3.7) although perhaps is still too low for comfort. We have also seen hints that the MV model may be in trouble with large scale structure and weak lensing measurements. Also, the overall goodness of fits of our model to both the supernovae and the WMAP data is not as good as the Λ CDM model. More work is needed in order to find whether it would be possible to overcome these potential problems by possibly modifying and/or adding new ingredients to the model. For instance, a primordial spectrum with a bump [15] (instead of running of the tilt as we considered here) as well as a 10% hot dark matter component [15, 16] seems already to overcome some of these difficulties. Although in these models the number of parameters is larger than what we consider, one obtains much better fits to the WMAP data (in fact, slightly better than Λ CDM). This “bump” model, in its original form, of course cannot reproduce the supernovae data, and the Hubble parameter ($h_{\text{out}} \sim 0.44$) is too low, so it seems natural to merge this model with our MV scenario. Another different possibility could be to add spatial curvature to the FLRW region. In fact we found that the goodness of fit to the WMAP data improves significantly, see table 4 for more details, even if we only include 5% in curvature. Finally, it may be that we have to look into larger voids, especially in trying to account for the LRG data (both galaxy power spectrum and the BAO peak).

We end with observational and theoretical possibilities of distinguishing the MV model from Λ CDM. The first logical way seems to be to perform galaxy counts up to very large distances and in a wide area in the sky, in order to directly check if we could really be living inside a huge Void. Secondly, there are features which can be checked by looking at SN Ia

themselves: firstly, the luminosity-redshift curve in the two models deviate from each other significantly at redshifts $z \geq 1$. Moreover, in the MV model the curve has a sharp peak (in correspondence with the boundary of the local region) around $z \simeq 0.1$, while this peak does not exist in the Λ CDM model. The up-coming experiment SDSS-II [23] will probably be able to discriminate the presence of such a peak. Another unique prediction for the MV model comes from realizing that the void is not expected to be exactly spherically symmetric, which could lead to detectable anisotropies in the Hubble parameter as well as in the low multipoles in CMB. Additionally, these anisotropies should be correlated! We note, also, that one could be able to constrain Voids by looking at the blackbody nature of the CMB [46, 47]. Our MV is still consistent with these constraints (while, according to [46], voids that extend up to $z \sim 1$ are excluded). Finally, studying large scale structure (as we plan to do in future work) one can study the compatibility of the primordial power spectrum we are assuming (with low tilt and large running, or with a bump) with the matter power spectrum. It may also be possible to test the existence of such a large running using Planck-satellite data as suggested by the Bayesian analysis performed in [48] using simulations.

In conclusion, we have shown that, for WMAP and SNIa observations, the MV model could be taken as an alternative to invoking a dark energy component that will be further tested in forthcoming supernovae observations. However, this should be only considered as a step towards trying to build an alternative to concordant Λ CDM cosmological model which has to be consistent with a host of other observations as well.

Note Added. Most of the above research work was completed before the release of the WMAP 5yr data and we have decided not to re-analyze the CMB data in the present paper for the following reason: although the 5-yr data improves the 3-yr data, there is no significant qualitative difference between the results presented in the 3-yr and 5-yr survey.

Acknowledgments

We would like to thank Robert Brandenberger, Paul Hunt, Subir Sarkar, Ravi Seth and Tarun Souradeep, for useful discussions and suggestions. We would specially like to thank Suman Bhattacharya, Jason Holmes and Antony Lewis for their help with COSMOMC. We thank Sebastian Szybka and Seshadri Nadathur for pointing out typos in earlier versions of the manuscript.

A Analytical results for LTB metric

A.1 Metric & density profile

In our paper we are interested in a special class of exact spherically symmetric solutions of Einstein’s equations with dust, known as the “open” LTB metric (in units $c = 1$). We follow the treatment given in ([3, 24]), where we have set the “mass function” to be cubic, which amounts to a redefinition of the radial coordinate (which is always possible if the mass function is a growing function of r). The metric is given by:

$$ds^2 = -dt^2 + S^2(r, t)dr^2 + R^2(r, t)(d\theta^2 + \sin^2 \theta d\varphi^2), \quad (\text{A.1})$$

Here we have employed comoving coordinates (r, θ, φ) and proper time t . The functions $S^2(r, t)$ and the dust density $\rho(r, t)$ is given in terms of $R(r, t)$ via

$$S^2(r, t) = \frac{R'^2(r, t)}{1 + 2(\bar{M}r)^2 k(r)}, \quad (\text{A.2})$$

$$\rho(r, t) = \frac{\bar{M}^2 M_p^2 r^2}{R'(r, t) R^2(r, t)}, \quad (\text{A.3})$$

where a dot denotes partial differentiation with respect to t and a prime with respect to r , while the function $R(r, t)$ itself is given implicitly as a function of (r, t) via an auxiliary variable $u(r, t)$:

$$R(r, t) = \frac{2\pi r}{3k(r)} (\cosh u - 1), \quad (\text{A.4})$$

$$\tau^3 \equiv \bar{M}t = \frac{\pi\sqrt{2}}{3k(r)^{3/2}} (\sinh u - u), \quad (\text{A.5})$$

In the above expressions, the ‘‘curvature’’ function $k(r)$ is left arbitrary (except that $k(r) \geq 0$) and this is what controls the density profile inside the LTB patch, while \bar{M} is just an arbitrary (unphysical) mass scale. Also, we have introduced the dimensionless conformal time τ for later convenience.

We also note that the average density inside the LTB patch is equal to the outside FLRW density (see for instance [3, 24]), in the limit in which we can neglect $(\bar{M}r)^2 k(r)$ in eq. (A.2) in the spatial metric when defining the average (in our case the correction is always negligible).

To get an intuitive and analytical understanding of how the density profile is related to the curvature function it is instructive to look at the ‘‘small- u ’’ approximation where we only keep next-to-leading terms in eq. (A.4) and eq. (A.5). This gives us eq. (2.1).

A.2 Photon trajectories

In order to perform supernovae fits we need to compute the luminosity (or angular) distances and redshifts for a photon trajectory emanating (backwards in time) from the central observer. The first step in this direction is to solve for the photon trajectory:

$$ds^2 = 0 \Rightarrow \frac{dt(r)}{dr} = -\frac{R'(r, t(r))}{\sqrt{1 + 2(\bar{M}r)^2 k(r)}}. \quad (\text{A.6})$$

The negative sign in front takes care of the fact that the time increases as the photons go towards the center. Analytical progress in solving the above equation is possible by realizing two things. Firstly, all quantities $(t(r), z(r), D_L(r))$ can be expressed as a power series in, $\bar{M}r \sim r/R_H$, and since this is a small quantity for the relevant inhomogeneous patches, we can just keep the next-to-leading order terms in these expansions [24]. Secondly, formally one can combine eq. (A.4) and eq. (A.5) to give us a power series expansion for $R(r, t)$ explicitly in terms of (r, t) [24]:

$$R(r, t) = \frac{1}{3}\pi\gamma^2 r\tau^2 (1 + R_2 u_0^2 + R_4 u_0^4 + \dots) \equiv \frac{1}{3}\pi\gamma^2 r\tau^2 (1 + f(u_0^2)), \quad (\text{A.7})$$

where

$$u_0 \equiv \gamma(\bar{M}t)^{1/3} \sqrt{k(r)} \text{ and } \gamma \equiv \left(\frac{9\sqrt{2}}{\pi}\right)^{1/3}. \quad (\text{A.8})$$

It is important to realize that the coefficients $\{R_n\}$, and hence the function f are universal (do not depend on the specific curvature function). It is implicitly defined via

$$1 + f(u_0^2) \equiv \frac{2(\cosh u - 1)}{u_0^2} \quad \text{and} \quad 6(\sinh u - u) = u_0^3. \quad (\text{A.9})$$

This is what allows us analyze the problem in its full generality.

It is convenient to recast the equation in terms of the conformal time, τ , and the dimensionless radial coordinate

$$\bar{r} = \bar{M}r. \quad (\text{A.10})$$

Substituting eq. (A.7) in eq. (A.6) one finds

$$\frac{d\tau}{d\bar{r}} = -\frac{\frac{\pi}{9}\gamma^2 \left[1 + \sum_1^\infty R_{2n}\gamma^{2n}\tau^{2n}(\bar{r}k^n)'\right]}{\sqrt{1 + 2k\bar{r}^2}}. \quad (\text{A.11})$$

The prime now denotes differentiation with respect to the rescaled \bar{r} . This can now be solved perturbative in \bar{r} to give us

$$\tau = \left(\tau_0 - \frac{\pi}{9}\gamma^2\bar{r}\right) - \frac{\pi}{9}\gamma^2\bar{r} \sum_1^\infty R_{2n}\gamma^{2n}\tau_0^{2n}k^n(\bar{r}) + \mathcal{O}(\bar{r}^2). \quad (\text{A.12})$$

The first two terms within the brackets corresponds to the FLRW expression for the trajectory while the rest of the terms give us the largest corrections coming from the inhomogeneities within a local patch. For corrections outside the patch see [24]. By comparing with eq. (A.7) the above expression can succinctly be written as

$$\tau(\bar{r}) = \tau_F(\bar{r}) - \frac{\pi}{9}\gamma^2\bar{r}f(\gamma^2\tau_0^2k(\bar{r})), \quad (\text{A.13})$$

where the subscript F corresponds to FLRW.

A.3 Luminosity distance vs. redshift

Having found the photon trajectory, the next step is to compute the redshift which is governed by the differential equation [2]

$$\frac{dz}{dr} = \frac{(1+z)\dot{R}'}{\sqrt{1 + 2k\bar{r}^2}}. \quad (\text{A.14})$$

Again, if we are only interested in computing corrections up to linear order in \bar{r} , then the redshift is given by

$$\int \frac{dz}{1+z} \approx \frac{2\pi\gamma^2}{9} \int \frac{d\bar{r}}{\tau} \left[1 + \sum_n (n+1)R_n\gamma^{2n}\tau^{2n}(rk^n)'\right] = \frac{2\pi\gamma^2}{9} \int \left[\frac{d\bar{r}}{\tau} + d\bar{r} \sum_n (n+1)R_n\gamma^{2n}\tau^{2n-1}(rk^n)'\right]. \quad (\text{A.15})$$

To evaluate the first integral we note that we can replace τ by τ_F as we will only be making an $\mathcal{O}(\bar{r}^2)$ error. Thus we have

$$\int \frac{d\bar{r}}{\tau} \approx \int \frac{d\bar{r}}{\tau_F} = -\frac{9}{\pi\gamma^2} \int \frac{d\tau_F}{\tau_F} = -\frac{9\gamma^2}{\pi} \ln \frac{\tau_F}{\tau_0}$$

The second term can be integrated straight forwardly up to linear terms in \bar{r} :

$$\begin{aligned} \sum_n (n+1) R_n \gamma^{2n} \int \tau^{2n-1} (r k^n)' d\bar{r} &\approx \sum_n (n+1) R_n \gamma^{2n} \tau_0^{2n-1} \int (\bar{r} k^n)' d\bar{r} \\ &= \sum_n (n+1) R_n \gamma^{2n} \tau_0^{2n-1} \bar{r} k^n \\ &= \bar{r} [f(\gamma^2 \tau_0^2 k(r)) + \gamma^2 \tau_0^2 k(r) f_1(\gamma^2 \tau_0^2 k(r))] / \tau_0 \end{aligned}$$

where we have defined

$$f_1(x) \equiv \frac{df(x)}{dx} \quad (\text{A.16})$$

Putting everything together we have

$$1+z = \left[\frac{\tau_0}{\tau_F(\bar{r})} \right]^2 \exp \left\{ \frac{2\pi\gamma^2\bar{r} [f(\gamma^2\tau_0^2 k(r)) + \gamma^2\tau_0^2 k(r) f_1(\gamma^2\tau_0^2 k(r))]}{9\tau_0} \right\}. \quad (\text{A.17})$$

Thus we have obtained an analytical approximation for the redshift as a function of the radial coordinate. We note in passing that the term in front of the exponential precisely correspond to the FLRW result. The corrections come from the exponential. In fact for small z one finds

$$z \approx \frac{2\pi}{9\tau_0} \gamma^2 \bar{r} [1 + f(\gamma^2 \tau_0^2 k(r)) + \gamma^2 \tau_0^2 k(r) f_1(\gamma^2 \tau_0^2 k(r))]. \quad (\text{A.18})$$

The luminosity distance, in General Theory of Relativity, is related to the angular diameter distance, D_A via

$$D_L = (1+z)^2 D_A. \quad (\text{A.19})$$

Now, in an LTB model when the observer is sitting at the center, the angular distance is simply given by

$$D_A = R = \frac{1}{3} \pi \gamma^2 r \tau^2 (1 + f(\gamma^2 \tau_0^2 k(\bar{r}))). \quad (\text{A.20})$$

Thus we now have both the luminosity distance and the redshift as a function of the radial coordinate and one can easily plot $D_L(z)$ and check whether the local void model can provide a good fit to the supernova data or not.

A.4 The ‘‘Jump’’

A particularly important quantity that can be inferred from the $D_L(z)$ curve is the jump parameter, $\mathcal{J} \equiv h/h_{\text{out}}$. Surprisingly, this turns out to not depend on the specific profiles, let us here see this analytically. First observe that since k' vanishes at $r=0$, we have the general result

$$R'(0, t) = \frac{1}{3} \pi \gamma^2 \tau_0^2 (1 + f_0), \quad (\text{A.21})$$

where f_0 corresponds to the value of f at $r=0$. Then using the exact expression for the density function eq. (A.3) one finds

$$\rho(r, t) = \frac{M_p^2}{6\pi t_0^2 (1 + f_0)^3}. \quad (\text{A.22})$$

The underdensity contrast at the center, δ_0 now can be easily related to f_0 :

$$\delta_0 = (1 + f_0)^{-3} - 1 \Rightarrow 1 + f_0 = (1 + \delta_0)^{-1/3}. \quad (\text{A.23})$$

Now, on the other hand using the definition of the Hubble parameter eq. (3.3), the correction to the redshift eq. (A.18), and the luminosity distance eq. (A.20) one finds

$$H_0^{-1} = H_{\text{out}}^{-1} \frac{1 + f_0}{1 + f_0 + u_0^2 f_{1,0}}.$$

Or in other words

$$\mathcal{J} = \frac{h}{h_{\text{out}}} = \frac{1 + f_0 + u_0^2 f_{1,0}}{1 + f_0}. \quad (\text{A.24})$$

Since δ_0 uniquely determines f_0 via (A.23), and $f(u_0^2)$ is a given function, it also determines u_0^2 and $f_{1,0} \equiv f_1(u_0^2)$. Thus in turn it also determines the jump parameter uniquely.

A.5 CMB dipole moment

Let us consider our observer to be located slightly off-center, at $r = r_O$. In this case the non-zero radial velocity of the observer will contribute towards a dipole moment in CMB:

$$\frac{\delta T}{T} \sim v_O = \dot{d}_O, \quad (\text{A.25})$$

where the proper radial distance, d_O , of the observer is given by

$$d_O = \int_0^{r_O} dr \frac{R'}{\sqrt{1 + 2(\bar{M}r)^2 k(r)}}$$

Now, in our profile $k(r)$ remains almost a constant for almost the entire underdense region. Assuming we are living in this ‘‘constant’’ underdense region, we have

$$d_O = \frac{2\pi(\cosh u - 1)}{3k_{\text{max}}} \int_0^{r_O} \frac{dr}{\sqrt{1 + 2(\bar{M}r)^2 k_{\text{max}}}} = \frac{2\pi(\cosh u - 1) \sinh^{-1}(\bar{M}\sqrt{2k_{\text{max}}}r_O)}{3k_{\text{max}}\bar{M}\sqrt{2k_{\text{max}}}}$$

(The simplification occurs because u and hence R' becomes only a function of time.) Further, since $\bar{M}r_O$ is expected to be very small, we have

$$d_O = \frac{2\pi(\cosh u - 1)r_O}{3k_{\text{max}}}. \quad (\text{A.26})$$

Taking the time derivative and simplifying we find

$$\dot{d}_O = \frac{d_O H_{\text{out}}}{4} \frac{u_0^3 \sinh u}{(\cosh u - 1)^2}. \quad (\text{A.27})$$

We now note that $u(u_0)$ is a known function eq. (A.9), in turn u_0 is known in terms of δ_0 via the function $f(u_0^2)$, see eq. (A.23). Thus, in principle, the second term in the right hand side of eq. (A.27) is determined in terms of the central underdensity contrast. Also, since the measured value of the CMB dipole moment $\sim 10^{-3}$, naturalness arguments suggest \dot{d}_O to be of the same order, and thus we have (after some simplifications):

$$d_O H_{\text{out}} \sim 10^{-3} \frac{\sqrt{2}(1 + f_0)^2}{\sqrt{u_0^2(1 + f_0)^2 + 2(1 + f_0)}}. \quad (\text{A.28})$$

For voids of around $200/h$ Mpc, and central underdensity contrasts between 40% and 50%, the dipole constraint eq. (A.28) typically imply that ‘‘we’’ have to be located within 10% of the void radius.

A.6 Analytic expression for the $D_L - z$ curve

In this subsection we wish to provide the reader a self-consistent summary of all the equations which are needed to plot the $D_L - z$ curve, in an analytic form. Following this, a fit of any experimental dataset can easily be performed. Here is the set of equations, which give D_L and z as a function of the radial coordinate r (therefore implicitly $D_L - z$). First of all one needs to define the function $f(u_0^2)$, implicitly given by:

$$f \equiv \frac{\sqrt[3]{2}(\cosh(u) - 1)}{3^{2/3}(\sinh(u) - u)^{2/3}} - 1 \quad (\text{A.29})$$

$$u_0 = 6^{1/3}(\sinh(u) - u)^{1/3}. \quad (\text{A.30})$$

Then, one can use this function in the following equations:

$$\tau(r) = \tau_0 - \frac{\pi}{9}\gamma^2\bar{M}r[1 + f(\gamma^2\tau_0^2k(r))], \quad (\text{A.31})$$

$$1 + z(r) = \left(\frac{\tau_0}{\tau(r)}\right)^2 \exp\left[\frac{4\pi\gamma^2\bar{M}r}{9}f(\gamma^2\tau_0^2k(r))\right] \quad (\text{A.32})$$

$$D_L(r) = \frac{\pi}{3}\gamma^2r\tau(r)^2[1 + f(\gamma^2\tau_0^2k(r))][1 + z(r)]^2 \quad (\text{A.33})$$

$$\tau_0 = \left(\frac{2\bar{M}}{3H_{\text{out}}}\right)^{1/3} \quad (\text{A.34})$$

$$\gamma = \left(\frac{9\sqrt{2}}{\pi}\right)^{1/3} \quad (\text{A.35})$$

The above formulas are completely general for any LTB profile, but we now focus into our specific one given by

$$k(r) = k_{\text{max}} \left[1 - \left(\frac{r}{L}\right)^4\right]^2. \quad (\text{A.36})$$

Then one has to choose appropriate values for H_0 , and for the length units for the coordinate r (given by \bar{M}). A simple choice is to set:

$$\sqrt{\frac{8\pi}{3}}\bar{M} = H_{\text{out}} = h_{\text{out}}/3000, \quad (\text{A.37})$$

where we have chosen, in this way, the units $\text{Mpc}=1$ (which turns out to be a convenient choice for the problem). Once this is done the physical parameter L (the radius of the patch) is approximately given already in Mpc . The comparison between the obtained curve and the fully numerical curve is shown in figure 6.

Finally the reader may play with the two parameters: the size L and k_{max} (which sets the amplitude of the density contrast). We also recall that the density profile is given by eq. (2.1) and that k_{max} can be directly related to the density contrast δ_0 at the center of the void at the present time, via the following equation:

$$\delta_0 = [1 + f(\gamma^2\tau_0^2k_{\text{max}})]^{-3} - 1. \quad (\text{A.38})$$

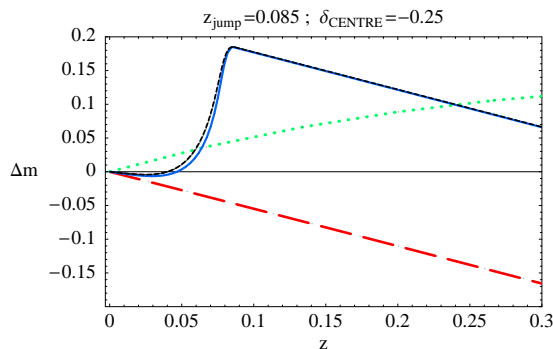


Figure 6. Comparison between analytic and numerical $D_L - z$ curves. The numerical curve is the blue solid line, the analytic approximation is the black short-dashed line. We have plotted also the EdS curve (red long-dashed line) and the Λ CDM, with $\Omega_\Lambda = 0.7$ (green dotted line). We have used the value $L = 400$, with the units given in eq. (A.37), and $k_{\max} = 2.2$ (which corresponds to a density contrast at the center $\delta_0 = -0.25$).

References

- [1] K. Tomita, *Distances and lensing in cosmological void models*, *Astrophys. J.* **529** (2000) 38 [[astro-ph/9906027](#)] [[SPIRES](#)]; *A Local Void and the Accelerating Universe*, *Mon. Not. Roy. Astron. Soc.* **326** (2001) 287 [[astro-ph/0011484](#)] [[SPIRES](#)]; *Analyses of Type Ia Supernova Data in Cosmological Models with a Local Void*, *Prog. Theor. Phys.* **106** (2001) 929 [[astro-ph/0104141](#)] [[SPIRES](#)]; *Distances and lensing in cosmological void models*, *Astrophys. J.* **529** (2000) 38 [[astro-ph/9906027](#)] [[SPIRES](#)]; *Luminous Matter Distribution, Bulk Flows and Baryon Contents in Cosmological Models with a Local Void*, *Prog. Theor. Phys.* **108** (2002) 103 [[astro-ph/0203125](#)] [[SPIRES](#)]; J.W. Moffat, *Cosmic Microwave Background, Accelerating Universe and Inhomogeneous Cosmology*, *JCAP* **10** (2005) 012 [[astro-ph/0502110](#)] [[SPIRES](#)]; *Late-time inhomogeneity and acceleration without dark energy*, *JCAP* **05** (2006) 001 [[astro-ph/0505326](#)] [[SPIRES](#)]; R. Mansouri, *Structured FRW universe leads to acceleration: A non-perturbative approach*, [[astro-ph/0512605](#)] [[SPIRES](#)]; H. Alnes, M. Amarzguioui and O. Gron, *An inhomogeneous alternative to dark energy?*, *Phys. Rev. D* **73** (2006) 083519 [[astro-ph/0512006](#)] [[SPIRES](#)]; D.J.H. Chung and A.E. Romano, *Mapping Luminosity-Redshift Relationship to LTB Cosmology*, *Phys. Rev. D* **74** (2006) 103507 [[astro-ph/0608403](#)] [[SPIRES](#)].
- [2] M.-N. Celerier, *Do we really see a cosmological constant in the supernovae data?*, *Astron. Astrophys.* **353** (2000) 63 [[astro-ph/9907206](#)] [[SPIRES](#)].
- [3] T. Biswas, R. Mansouri and A. Notari, *Nonlinear Structure Formation and Apparent Acceleration: an Investigation*, *JCAP* **12** (2007) 017 [[astro-ph/0606703](#)] [[SPIRES](#)].
- [4] M.-N. Celerier, *The Accelerated Expansion of the Universe Challenged by an Effect of the Inhomogeneities. A Review*, [[astro-ph/0702416](#)] [[SPIRES](#)].
- [5] S.F. Shandarin, J.V. Sheth and V. Sahni, *Morphology of the supercluster-void network in LCDM cosmology*, *Mon. Not. Roy. Astron. Soc.* **353** (2004) 162 [[astro-ph/0312110](#)] [[SPIRES](#)].
- [6] J.R.I. Gott et al., *A Map of the Universe*, *Astrophys. J.* **624** (2005) 463 [[astro-ph/0310571](#)] [[SPIRES](#)].
- [7] W.J. Frith, G.S. Buswell, R. Fong, N. Metcalfe and T. Shanks, *The Local Hole in the Galaxy Distribution: Evidence from 2MASS*, *Mon. Not. Roy. Astron. Soc.* **345** (2003) 1049 [[astro-ph/0302331](#)] [[SPIRES](#)].

- [8] M. Cruz, M. Tucci, E. Martinez-Gonzalez and P. Vielva, *The non-Gaussian Cold Spot in WMAP: significance, morphology and foreground contribution*, *Mon. Not. Roy. Astron. Soc.* **369** (2006) 57 [[astro-ph/0601427](#)] [[SPIRES](#)];
M. Cruz, L. Cayon, E. Martinez-Gonzalez, P. Vielva and J. Jin, *The non-Gaussian Cold Spot in the 3-year WMAP data*, *Astrophys. J.* **655** (2007) 11 [[astro-ph/0603859](#)] [[SPIRES](#)].
- [9] L. Rudnick, S. Brown and L.R. Williams, *Extragalactic Radio Sources and the WMAP Cold Spot*, *Astrophys. J.* **671** (2007) 40 [[arXiv:0704.0908](#)] [[SPIRES](#)].
- [10] K.T. Inoue and J. Silk, *Local Voids as the Origin of Large-angle Cosmic Microwave Background Anomalies: The Effect of a Cosmological Constant*, *Astrophys. J.* **664** (2007) 650 [[astro-ph/0612347](#)] [[SPIRES](#)]; *Local Voids as the Origin of Large-angle Cosmic Microwave Background Anomalies*, *Astrophys. J.* **648** (2006) 23 [[astro-ph/0602478](#)] [[SPIRES](#)].
- [11] D.J. Schwarz and B. Weinhorst, *(An)isotropy of the Hubble diagram: comparing hemispheres*, [arXiv:0706.0165](#) [[SPIRES](#)].
- [12] M.L. McClure and C.C. Dyer, *Anisotropy in the Hubble constant as observed in the HST Extragalactic Distance Scale Key Project results*, *New Astron.* **12** (2007) 533 [[astro-ph/0703556](#)] [[SPIRES](#)].
- [13] K. Tomita, *Anisotropy of the Hubble Constant in a Cosmological Model with a Local Void on Scales of ~ 200 Mpc*, *Prog. Theor. Phys.* **105** (2001) 419 [[astro-ph/0005031](#)] [[SPIRES](#)].
- [14] A. Lewis and S. Bridle, *Cosmological parameters from CMB and other data: a Monte-Carlo approach*, *Phys. Rev. D* **66** (2002) 103511 [[astro-ph/0205436](#)] [[SPIRES](#)]; <http://cosmologist.info/cosmomc/>.
- [15] P. Hunt and S. Sarkar, *Multiple inflation and the WMAP 'glitches' II. Data analysis and cosmological parameter extraction*, *Phys. Rev. D* **76** (2007) 123504 [[arXiv:0706.2443](#)] [[SPIRES](#)].
- [16] A. Blanchard, M. Douspis, M. Rowan-Robinson and S. Sarkar, *An alternative to the cosmological 'concordance model'*, *Astron. Astrophys.* **412** (2003) 35 [[astro-ph/0304237](#)] [[SPIRES](#)].
- [17] A. Shafieloo and T. Souradeep, *Estimation of Primordial Spectrum with post-WMAP 3 year data*, *Phys. Rev. D* **78** (2008) 023511 [[arXiv:0709.1944](#)] [[SPIRES](#)].
- [18] G. Lemaître, *L'Univers en expansion*, *Ann. soc. Sci. Bruxelles Ser. I* **A53** (1933) 51;
R.C. Tolman, *Effect of Inhomogeneity on Cosmological Models*, *Proc. Nat. Acad. Sci. U.S.A.* **20** (1934) 410;
H. Bondi, *Spherically symmetrical models in general relativity*, *Mon. Not. Roy. Astron. Soc.* **107** (1947) 343.
- [19] S. Khakshournia and R. Mansouri, *Dynamics of general relativistic spherically symmetric dust thick shells*, *Gen. Rel. Grav.* **34** (2002) 1847 [[gr-qc/0308025](#)] [[SPIRES](#)].
- [20] Y.B. Zeldovich, *Gravitational instability: An Approximate theory for large density perturbations*, *Astron. Astrophys.* **5** (1970) 84 [[SPIRES](#)].
- [21] HST collaboration, W.L. Freedman et al., *Final Results from the Hubble Space Telescope Key Project to Measure the Hubble Constant*, *Astrophys. J.* **553** (2001) 47 [[astro-ph/0012376](#)] [[SPIRES](#)].
- [22] A.G. Riess et al., *New Hubble Space Telescope Discoveries of Type Ia Supernovae at $z > 1$: Narrowing Constraints on the Early Behavior of Dark Energy*, *Astrophys. J.* **659** (2007) 98 [[astro-ph/0611572](#)] [[SPIRES](#)].
- [23] <http://sdssdp47.fnal.gov/sdsssn/sdsssn.html>.
- [24] T. Biswas and A. Notari, *Swiss-Cheese Inhomogeneous Cosmology & the Dark Energy Problem*, *JCAP* **06** (2008) 021 [[astro-ph/0702555](#)] [[SPIRES](#)].

- [25] V. Marra, E.W. Kolb, S. Matarrese and A. Riotto, *On cosmological observables in a swiss-cheese universe*, *Phys. Rev. D* **76** (2007) 123004 [[arXiv:0708.3622](#)] [[SPIRES](#)]; V. Marra, E.W. Kolb and S. Matarrese, *Light-cone averages in a swiss-cheese universe*, *Phys. Rev. D* **77** (2008) 023003 [[arXiv:0710.5505](#)] [[SPIRES](#)].
- [26] N. Brouzakis, N. Tetradis and E. Tzavara, *The Effect of Large-Scale Inhomogeneities on the Luminosity Distance*, *JCAP* **02** (2007) 013 [[astro-ph/0612179](#)] [[SPIRES](#)]; *Light Propagation and Large-Scale Inhomogeneities*, *JCAP* **04** (2008) 008 [[astro-ph/0703586](#)] [[SPIRES](#)].
- [27] S.M. Carroll, W.H. Press and E.L. Turner, *The Cosmological constant*, *Ann. Rev. Astron. Astrophys.* **30** (1992) 499 [[SPIRES](#)].
- [28] B.R. Parodi, A. Saha, A. Sandage and G.A. Tammann, *Supernova type-IA luminosities, their dependence on second parameters and the value of H_0* , *Astrophys. J.* **540** (1989) 634 [[astro-ph/0004063](#)] [[SPIRES](#)].
- [29] A. Sandage et al., *The Hubble Constant: A Summary of the HST Program for the Luminosity Calibration of Type Ia Supernovae by Means of Cepheids*, *Astrophys. J.* **653** (2006) 843 [[astro-ph/0603647](#)] [[SPIRES](#)].
- [30] E.D. Reese et al., *Determining the Cosmic Distance Scale from Interferometric Measurements of the Sunyaev-Zel'dovich Effect*, *Astrophys. J.* **581** (2002) 53 [[astro-ph/0205350](#)] [[SPIRES](#)]; J.E. Carlstrom, G.P. Holder and E.D. Reese, *Cosmology with the Sunyaev-Zel'dovich Effect*, *Ann. Rev. Astron. Astrophys.* **40** (2002) 643 [[astro-ph/0208192](#)] [[SPIRES](#)].
- [31] M. Bonamente et al., *Measurement of the cosmic distance scale from Chandra X-ray imaging and Sunyaev-Zel'dovich Effect mapping of high redshift clusters of galaxies*, [astro-ph/0512349](#) [[SPIRES](#)].
- [32] C.S. Kochanek and P.L. Schechter, *The Hubble constant from gravitational lens time delays*, [astro-ph/0306040](#) [[SPIRES](#)].
- [33] J.M.H. Etherington, *On the Definition of Distance in General Relativity*, *Phil. Mag.* **15** (1933) 761; G.F.R. Ellis, *Relativistic cosmology*, in *General Relativity and Cosmology*, *Proc. School "Enrico Fermi"*, Ed. R.K. Sachs, New York (1971).
- [34] ESSENCE collaboration, W.M. Wood-Vasey et al., *Observational Constraints on the Nature of the Dark Energy: First Cosmological Results from the ESSENCE Supernova Survey*, *Astrophys. J.* **666** (2007) 694 [[astro-ph/0701041](#)] [[SPIRES](#)].
- [35] H. Alnes and M. Amarzguioui, *CMB anisotropies seen by an off-center observer in a spherically symmetric inhomogeneous universe*, *Phys. Rev. D* **74** (2006) 103520 [[astro-ph/0607334](#)] [[SPIRES](#)].
- [36] P. Fosalba, E. Gaztanaga and F. Castander, *Detection of the ISW and SZ effects from the CMB-Galaxy correlation*, *Astrophys. J.* **597** (2003) L89 [[astro-ph/0307249](#)] [[SPIRES](#)]; S. Boughn and R. Crittenden, *A correlation of the cosmic microwave sky with large scale structure*, *Nature* **427** (2004) 45 [[astro-ph/0305001](#)] [[SPIRES](#)]; T. Giannantonio et al., *A high redshift detection of the integrated Sachs-Wolfe effect*, *Phys. Rev. D* **74** (2006) 063520 [[astro-ph/0607572](#)] [[SPIRES](#)]; D. Pietrobon, A. Balbi and D. Marinucci, *Integrated Sachs-Wolfe effect from the cross-correlation of WMAP 3 year and NVSS: new results and constraints on dark energy*, *Phys. Rev. D* **74** (2006) 043524 [[astro-ph/0606475](#)] [[SPIRES](#)]; J.D. McEwen, P. Vielva, M.P. Hobson, E. Martinez-Gonzalez and A.N. Lasenby, *Detection of the ISW effect and corresponding dark energy constraints made with directional spherical wavelets*, *Mon. Not. Roy. Astron. Soc.* **373** (2007) 1211 [[astro-ph/0602398](#)] [[SPIRES](#)]; A. Rassat, K. Land, O. Lahav and F.B. Abdalla, *Cross-correlation of 2MASS and WMAP3: Implications for the Integrated Sachs-Wolfe effect*, *Mon. Not. Roy. Astron. Soc.* **377** (2007) 1085 [[astro-ph/0610911](#)] [[SPIRES](#)].

- [37] B. Fields and S. Sarkar, *Big-bang nucleosynthesis (PDG mini-review)*, [astro-ph/0601514](#) [SPIRES].
- [38] F. Di Marco and A. Notari, 'Graceful' old inflation, *Phys. Rev. D* **73** (2006) 063514 [[astro-ph/0511396](#)] [SPIRES];
T. Biswas and A. Notari, *Can inflation solve the hierarchy problem?*, *Phys. Rev. D* **74** (2006) 043508 [[hep-ph/0511207](#)] [SPIRES].
- [39] T. Biswas, R. Brandenberger, D.A. Easson and A. Mazumdar, *Coupled inflation and brane gases*, *Phys. Rev. D* **71** (2005) 083514 [[hep-th/0501194](#)] [SPIRES].
- [40] A. Blanchard, M. Douspis, M. Rowan-Robinson and S. Sarkar, *Large-scale galaxy correlations as a test for dark energy*, *Astron. Astrophys.* **449** (2006) 925 [[astro-ph/0512085](#)] [SPIRES];
- [41] SDSS collaboration, D.J. Eisenstein et al., *Detection of the Baryon Acoustic Peak in the Large-Scale Correlation Function of SDSS Luminous Red Galaxies*, *Astrophys. J.* **633** (2005) 560 [[astro-ph/0501171](#)] [SPIRES].
- [42] J. Lesgourgues, M. Viel, M.G. Haehnelt and R. Massey, *A Combined analysis of Lyman-alpha forest, 3D Weak Lensing and WMAP year three data*, *JCAP* **11** (2007) 008 [[arXiv:0705.0533](#)] [SPIRES].
- [43] J.P. Zibin, *Scalar Perturbations on Lemaitre-Tolman-Bondi Spacetimes*, *Phys. Rev. D* **78** (2008) 043504 [[arXiv:0804.1787](#)] [SPIRES].
- [44] R. Cen, *Implications of WMAP Observations On the Population III Star Formation Processes*, *Astrophys. J.* **591** (2003) L5 [[astro-ph/0303236](#)] [SPIRES];
B. Ciardi, A. Ferrara and S.D.M. White, *Early Reionization by the First Galaxies*, *Mon. Not. Roy. Astron. Soc.* **344** (2003) L7 [[astro-ph/0302451](#)] [SPIRES];
Z. Haiman and G.P. Holder, *The Reionization History at High Redshifts I: Physical Models and New Constraints from CMB Polarization*, *Astrophys. J.* **595** (2003) 1 [[astro-ph/0302403](#)] [SPIRES];
P. Madau, M.J. Rees, M. Volonteri, F. Haardt and S.P. Oh, *Early reionization by miniquasars*, *Astrophys. J.* **604** (2004) 484 [[astro-ph/0310223](#)] [SPIRES];
S.P. Oh and Z. Haiman, *Fossil HII Regions: Self-Limiting Star Formation at High Redshift*, *Mon. Not. Roy. Astron. Soc.* **346** (2003) 456 [[astro-ph/0307135](#)] [SPIRES];
M. Ricotti and J.P. Ostriker, *X-ray Preionisation Powered by Accretion on the First Black Holes. I: a Model for the WMAP Polarisation Measurement*, *Mon. Not. Roy. Astron. Soc.* **352** (2004) 547 [[astro-ph/0311003](#)] [SPIRES];
A. Sokasian, N. Yoshida, T. Abel, L. Hernquist and V. Springel, *Cosmic Reionisation by Stellar Sources: Population III Stars*, *Mon. Not. Roy. Astron. Soc.* **350** (2004) 47 [[astro-ph/0307451](#)] [SPIRES];
R.S. Somerville and M. Livio, *Star Formation at the Twilight of the Dark Ages: Which Stars Reionized the Universe?*, *Astrophys. J.* **593** (2003) 611 [[astro-ph/0303017](#)] [SPIRES];
I.T. Iliev et al., *Simulating Cosmic Reionization at Large Scales I: the Geometry of Reionization*, *Mon. Not. Roy. Astron. Soc.* **369** (2006) 1625 [[astro-ph/0512187](#)] [SPIRES].
- [45] WMAP collaboration, D.N. Spergel et al., *Wilkinson Microwave Anisotropy Probe (WMAP) three year results: Implications for cosmology*, *Astrophys. J. Suppl.* **170** (2007) 377 [[astro-ph/0603449](#)] [SPIRES].
- [46] R.R. Caldwell and A. Stebbins, *A Test of the Copernican Principle*, *Phys. Rev. Lett.* **100** (2008) 191302 [[arXiv:0711.3459](#)] [SPIRES].
- [47] J. Goodman, *Geocentrism reexamined*, *Phys. Rev. D* **52** (1995) 1821 [[astro-ph/9506068](#)] [SPIRES].
- [48] C. Pahud, A.R. Liddle, P. Mukherjee and D. Parkinson, *When can the Planck satellite measure spectral index running?*, *Mon. Not. Roy. Astron. Soc.* **381** (2007) 489 [[astro-ph/0701481](#)] [SPIRES].